High temperature characteristics of bilayer epitaxial graphene field-effect transistors on SiC Substrate*

Ze-Zhao He(何泽召)[1,2], Ke-Wu Yang(杨克武)[1,2], Cui Yu(蔚翠)[2], Qing-Bin Liu(刘庆彬)[2], Jing-Jing Wang(王晶晶)[2], Jia Li(李佳)[2], Wei-Li Lu(芦伟立)[2], Zhi-Hong Feng(冯志红)[2,†], and Shu-Jun Cai(蔡树军)[2]

[1] *School of Electronic and Information Engineering, Hebei University of Technology, Tianjin* 300130, *China*
[2] *National Key Laboratory of ASIC, Hebei Semiconductor Research Institute, Shijiazhuang* 050051, *China*

(Received 1 February 2016; revised manuscript received 10 March 2016; published online 25 May 2016)

In this paper, high temperature direct current (DC) performance of bilayer epitaxial graphene device on SiC substrate is studied in a temperature range from 25 °C to 200 °C. At a gate voltage of −8 V (far from Dirac point), the drain-source current decreases obviously with increasing temperature, but it has little change at a gate bias of +8 V (near Dirac point). The competing interactions between scattering and thermal activation are responsible for the different reduction tendencies. Four different kinds of scatterings are taken into account to qualitatively analyze the carrier mobility under different temperatures. The devices exhibit almost unchanged DC performances after high temperature measurements at 200 °C for 5 hours in air ambience, demonstrating the high thermal stabilities of the bilayer epitaxial graphene devices.

Keywords: epitaxial graphene, field-effect transistor, high temperature characteristics

PACS: 72.80.Vp, 65.80.Ck, 68.65.Pq **DOI:** 10.1088/1674-1056/25/6/067206

1. Introduction

Graphene has attracted significant attention as a potential emerging semiconductor material for future electronics due to its excellent physical and electrical properties, such as the outstanding carrier mobility, high current density, large mechanical strength, excellent thermal conductivity, etc.[1–3] Over the past ten years, a number of advances in graphene based devices have been made. A intrinsic cutoff frequency (f_T) of 427 GHz with 67-nm gate length graphene field-effect transistor (GFET) has been reported for peeled graphene.[4] Recently, 100-nm gate length epitaxial graphene transistor fabricated on SiC substrate has exhibited an intrinsic f_{max} of 137 GHz.[5] Several other significant efforts have also been made to improve the device performance and develop new graphene-based applications,[6–9] such as graphene nanoribbons, terahertz devices, photodetectors, and other graphene-based devices and circuits. In practical applications, however, graphene devices demand not only good operation performances but also thermal stabilities. Thermal effects, including self-heating generated during device operation and ambient temperature variations, will strongly affect the characteristics of devices, leading to degradations of device performances. Therefore it is very important to understand the operation mechanisms of graphene devices at different temperatures.

Many groups have reported on the temperature dependent characteristics of graphene devices at relatively low temperatures, typically ranging from ∼1.5 K to 380 K.[10–12] For example, Bolotin *et al.* investigated the temperature-dependent transport in suspended graphene in a temperature range 5 K < T < 240 K.[11] Feng *et al.* studied the temperature-dependent electrical properties of GFETs in ambient atmosphere with temperature rising from 300 K to 380 K.[12] These early studies gave an insight into the understanding of the basic physical and electronic properties of graphene. In many practical applications, devices often work under different kinds of high temperature conditions, such as the temperature above 100 °C. It is important to investigate the behaviors of graphene devices under high temperature. But few reports on high temperature performances of graphene devices can be found in the literature.

In this work, bilayer epitaxial GFETs are fabricated on 4H–SiC substrate. The DC performances of graphene devices are studied at the temperatures ranging from 25 °C to 200 °C. The operation mechanisms and thermal stabilities of GFETs under high temperature are investigated.

2. Experiment

Epitaxial graphene layers were synthesized on 10 mm × 10 mm semi-insulating Si-face 4H–SiC (0001) substrates. Prior to the graphene growth, the substrates were hydrogen etched at 1650 °C to form a regularly stepped surface. Mono-

*Project supported by the National Natural Science Foundation of China (Grant No. 61306006).
†Corresponding author. E-mail: ga917vv@163.com
© 2016 Chinese Physical Society and IOP Publishing Ltd

layer graphene was grown on the SiC substrate in Ar ambient at 1650 °C. Then, the as-grown graphene was annealed in molecular hydrogen atmosphere at 900 °C, which can result in the formation of the bilayer quasi-free-standing epitaxial graphene (QFSEG). More details of the growth can be found in our early work.[13,14] The as-grown bilayer epitaxial graphene shows p-type doping with carrier density $n_s = 1.41 \times 10^{13}$ cm^{-2}, Hall mobility $\mu = 3110$ cm^2/V·s, and sheet resistance $R_{sheet} = 142.3$ Ω/□. In this work, bilayer QFSEG was used to fabricate the graphene devices.

An improved device process is used to fabricate GFETs, in which an Au metal film was pre-deposited on graphene surface as a protection layer to avoid undesired damage and contamination to graphene during processing. A similar process flow can be found in our previous work[5,15] and is summarized as follows. First, a 20-nm Au metal film was deposited on the surface of bilayer epitaxial graphene on SiC substrate. Channel region was then patterned by optical lithography and Au film outside the channel was removed by KI-I_2 etchant solution. Electrical isolation was achieved by exposure of the graphene surface to oxygen plasma. The metal electrodes (Ti/Au, 10 nm/250 nm) were evaporated at the top of the Au film followed by a lift-off process. The exposed Au layer between metal electrodes was wet etched away to form the valid source/drain separations automatically. The devices were equipped in an electronbeam evaporator to deposit 2-nm Al nucleation layer. Then, 20-nm Al_2O_3 film was deposited on the surface of device via the Atomic layer deposition (ALD) at 250 °C. Rapid thermal annealing at 400 °C for 2 min in nitrogen was conducted to improve the quality of the Al_2O_3 film.[16] Finally a 250-nm Al top-gate electrode was thermally evaporated and a lift-off process was performed.

3. Results and discussion

Raman spectrum of bilayer epitaxial graphene on SiC substrate is shown in Fig. 1(a). The full width of half maximum (FWHM) of two-dimensional (2D) peak is ~59 cm^{-1}, and the 2D band can be divided into four Lorentzian sub-bands, which is the evidence for bilayer structure of graphene.[17] An inset of Fig. 1(a) shows the morphology of graphene surface characterized by atomic force microscopy (AFM), revealing smooth and wide terrace which is around 19 μm. Figure 1(b) shows a schematic diagram of top-gated GFET on SiC substrate. The device structure consists of a graphene channel that is gated through Al_2O_3 dielectric from the top gate. Optical microscope image of GFET is shown in Fig. 1(c) with a gate length (L_g) of 1.2 μm and a gate width (W_g) of 2 μm.

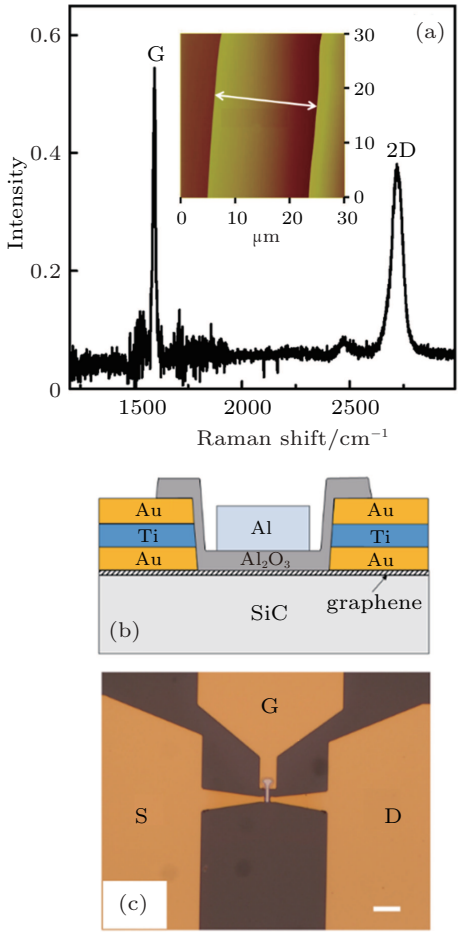


Fig. 1. (color online) (a) Raman spectrum of bilayer epitaxial graphene on 4H–SiC (0001). An inset shows the AFM image of bilayer graphene on SiC with a smooth terrace width of about 19 μm. The scanning area is 30 μm × 30 μm. (b) A schematic drawing of top-gated GFET. (c) Optical micrograph of top-gated GFET. The gate length (L_g) and gate width (W_g) are 1.2 μm and 2 μm, respectively. The scale bar is 10 μm.

Figures 2(a) and 2(b) show the variations of drain-source current (I_{DS}) with drain-source voltage (V_{DS}) scanned from 0 to −2 V for gate biases (V_G) ranging from −8 V to +8 V at different temperatures (from 25 °C to 200 °C in steps of 25 °C). The bilayer graphene device shows p-type characteristic. The maximum I_{DS} (defined at $V_{DS} = -2$ V and $V_G = -8$ V) decreases with increasing temperature and drops from 2.36 A/mm to 2.07 A/mm as temperature increases from 25 °C to 200 °C. When increasing the V_G to +8 V, the I_{DS} shows a weak temperature dependence, and the minimum I_{DS} ($V_{DS} = -2$ V, $V_G = +8$ V) shows no obvious change with temperature. Figure 2(c) shows the curves of transfer characteristics and g_m at $V_{DS} = -2$ V with V_G scanned from −8 V to +8 V at various temperatures. Both I_{DS} and g_m decrease with increasing temperature, indicating degeneration of device performance under high temperature environment. It is seen that at the V_G of −8 V, I_{DS} decreases obviously with the increase of temperature, but has little change at the V_G of +8 V (near the charge neutrality point), which is similar to the phenomenon as mentioned above in curves of I_{DS}–V_{DS}. To inves-

tigate the temperature-dependent I_{DS} of GFET over different values of V_G, the variations of I_{DS} are quantitatively calculated as shown in Fig. 2(d). The value of variation in I_{DS} is defined as $\theta = ((I_{DS-25\,^\circ C} - I_{DS-200\,^\circ C})/I_{DS-25\,^\circ C}) \times 100\%$. At the V_G of -8 V, a reduction of 12.58% is observed from 25 °C to 200 °C, while at the V_G of +8 V, the reduction is only as small as 0.88%. A similar phenomenon has been seen in several theoretical and experimental studies.[11,18,19] An inset in Fig. 2(d) shows the energy-band diagram of graphene with V_G swept from -8 V to +8 V. For graphene at high carrier density, the temperature-dependent scattering effect becomes prevailed, which leads to a metallic behavior ($\partial\sigma/\partial T < 0$, $\sigma = ne\mu$) of the graphene channel conductance. While in a low carrier density region (at or close to the Dirac point), thermal activation of charge carriers in electron-hole puddles originating from potential fluctuations associated with randomly distributed charged impurities plays a very important role, which gives rise to the increase of carrier density and results in a semiconducting behavior ($\partial\sigma/\partial T > 0$).

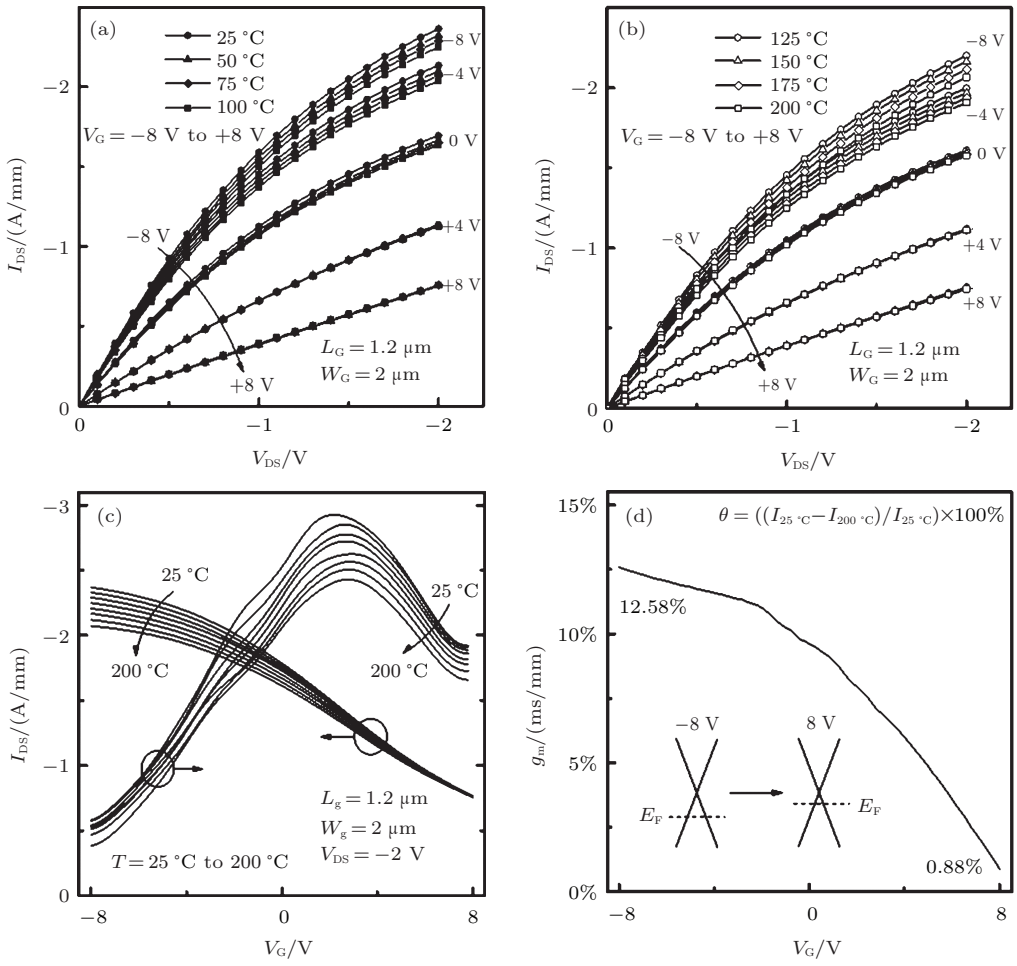


Fig. 2. (a) and (b) Temperature-dependent I_{DS}–V_{DS} characteristics of a GFET. (c) Temperature-dependent I_{DS}–V_G and g_m at $V_{DS} = -2$ V. (d) The calculated value of θ as a function of V_G for GFET. Inset shows the gate voltage dependence of Fermi level (E_F) of graphene.

For our device, when $V_G = -8$ V, a high carrier density regime is formed in the channel of graphene. Thermal activation of electron-hole puddles is exponentially suppressed at this time, and the scattering effect plays a major role and dominates the channel of graphene. Hence the I_{DS} $(\sigma \cdot E)$ of GFET decreases obviously with increasing temperature, and 12.58% reduction of I_{DS} is observed under 200 °C with $V_G = -8$ V. The gate voltage is scanned from negative to positive voltage, and the number of carriers in the channel is reduced, and I_{DS} shows a continuous drop with V_G increasing. At a V_G of +8 V, a relatively low carrier density regime is formed in the graphene channel and the thermal activation will dominate. It is needed to point out that to avoid the electrical breakdown of Al_2O_3 dielectric the bias applied to the gate does not exceed +8 V. The Dirac point is not reached in this measurement for our device. Dirac point is larger than +8 V, implying that the carrier density under V_G of +8 V is not low enough and a pure semiconducting behavior cannot be present here. It is observed in Fig. 2(d) that the I_{DS} shows a small reduction of 0.88% under a V_G of +8 V at a temperature of 200 °C. The reduction indicates that a weak metallic behavior is still maintained in the graphene channel. This phenomenon is the result of the

competing interactions between physical mechanisms of scattering and thermal activation, indicating that scattering has a stronger influence on the carrier of graphene than the thermal activation. Hence, only a little reduction of I_{DS} is observed under the condition of $V_G = +8$ V in the device.

It is important to note that the maximum I_{DS} of GFET is only reduced by 12.58% after the temperature increasing from 25 °C to 200 °C. This value of reduction in the GFET is significantly smaller than those of other traditional semiconductors (e.g., silicon, GaN, etc.) devices. It is reported that a very large reduction of about 61% for the maximum I_{DS} is observed in GaN-based MOSFET after the temperature rising from 25 °C to 200 °C.[20] To give an insight into the reasons for this small I_{DS} reduction, the temperature-dependent scattering effect is used to investigate the operation mechanisms of GFETs. I_{DS} can be determined using the following expression:

$$I_{DS} = \sigma \cdot E = n_s e \mu \cdot E, \tag{1}$$

where σ is the conductance of graphene channel, E is the electric field between drain-source electrodes, n_s is the carrier density, e is the charge of electron, and μ is the carrier mobility. For a fixed V_{DS}, I_{DS} is proportional to the product of n_s and μ. In our previous study, the carrier density n_s of bilayer QFSEG from Hall measurements (from 1.26×10^{13} cm^{-2} of 300 K to 1.28×10^{13} cm^{-2} of 500 K) showed a very slightly increase with temperature.[14] The n_s can be regarded as a constant which is independent of temperature. Then, I_{DS} can be described by a simplified formula as $I_{DS} = A_1 \cdot \mu_T$, where A_1 is the fitting parameter and μ_T is the mobility at different temperatures. It is well known that the carrier mobility is inextricably linked to the scattering. Here, four different scattering sources are considered: 1) μ_c, Coulomb scattering; 2) μ_{gr}, acoustic phonon scattering of graphene; 3) μ_{RP}, remote optical phonon scattering from SiC substrate and gate dielectric of Al_2O_3; 4) μ_{sr}, short range scattering, which can be approximately calculated by the following formulas for bilayer graphene, respectively:[13,14]

$$\mu_c = \frac{A + B \cdot T}{n_{imp}}, \tag{2}$$

where A and B are constants, T is the temperature, and n_{imp} is the impurity density;

$$\mu_{gr} = \frac{4e^2 \hbar \rho_s v_s^2 v_F^2}{\pi D_A^2 k_B} \frac{1}{n_s e} \frac{1}{T}, \tag{3}$$

where h is the reduced Planck's constant, ρ_s is the mass density of graphene (7.6×10^{-7} kg·m^{-2}), v_s is the LA phonon velocity (2.1×10^4 m·s^{-1}), V_F is the Fermi velocity ($\sim 1 \times 10^6$ m·s^1), D_A is the experimentally obtained deformation potential (18 eV), and k_B is the Boltzmann's constant;

$$\mu_{RP} = \left(\frac{C_{RP-SiC}}{e^{E_{op-SiC}/k_B T} - 1} + \frac{C_{RP-Al_2O_3}}{e^{E_{op1-Al_2O_3}/k_B T} - 1} + \frac{C_{RP-Al_2O_3}}{e^{E_{op1-Al_2O_3}/k_B T} - 1} \right)^{-1} \frac{1}{n_s e}, \tag{4}$$

where C_{RP-SiC} and $C_{RP-Al_2O_3}$ are the coupling strength E_{op} is the phonon energy coupled to the charge carriers in graphene, the values of E_{op-SiC}, $E_{op1-Al2O3}$, and $E_{op2-Al_2O_3}$ are 116 meV, 55.01 meV, and 94.29 meV, respectively;[21]

$$\mu_{sr} = S, \tag{5}$$

where S is a constant. The total carrier mobility μ can be regarded as the result of interaction among the four different scattering sources and is given by

$$\mu^{-1} = \mu_c^{-1} + \mu_{gr}^{-1} + \mu_{RP}^{-1} + \mu_{sr}^{-1}. \tag{6}$$

The temperature dependences of the four kinds of scatterings are different. The strength of short range scattering depends on the quality of the graphene sample. The μ_{sr} is a constant and temperature independent. The μ_c shows a proportional relationship with temperature. Owing to the parabolic band structure of the bilayer graphene, the energy averaging of the Coulomb scattering time can result in the mobility increasing proportionally with temperature. The acoustic phonon scattering of graphene is inversely proportional to temperature, which results in the mobility decreasing with temperature. The carrier in the graphene will also be scattered by optical phonons of SiC substrates and Al_2O_3 dielectric, which results in the mobility decreasing with temperature. The competition result between Coulomb scattering and acoustic phonon scattering of graphene, and the remote phonon (RP) scattering of substrates/dielectric cause a relatively small decrease of μ at high temperature, which leads to the slight reduction of I_{DS} in the GFETs. The above analysis indicates that the small decrease of μ at high temperature lies in the increase of Coulomb scattering mobility with temperature rising due to its parabolic band structure of bilayer graphene. The bilayer graphene transistors show some advantages in high temperature applications.

In order to further investigate the performance of GFET under high temperature, the thermal stability test is conducted in this work. The measurement is carried out under 200 °C in air ambience. The output characteristics of a GFET at different heating times are shown in Fig. 3(a). It is observed that the graphene device exhibits almost unchanged performance after high temperature measurements at 200 °C for 5 hours. Figure 3(b) shows the results of the maximal I_{DS} and g_m versus

time, demonstrating a long-term thermal stability for bilayer graphene device.

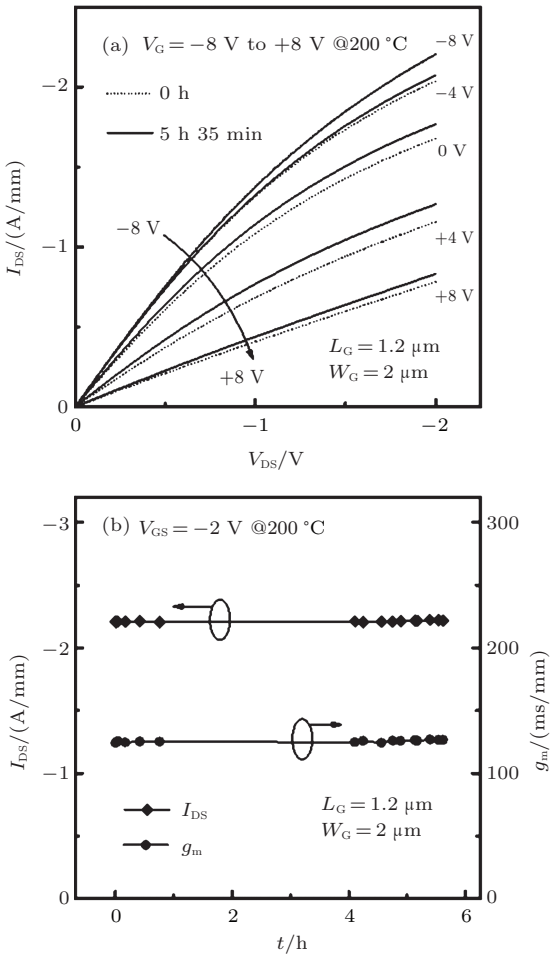


Fig. 3. (a) I_{DS}–V_{DS} characteristics of GFET for 0 hour and 5 hour 35 min latter under 200 °C in ambient. (b) The maximum I_{DS} and g_m versus time.

4. Conclusions

In this paper, high temperature DC performances of bilayer epitaxial graphene devices on SiC substrate are studied. When graphene channel has a high carrier density, the I_{DS} decreases obviously with temperature increasing, but it has little change when graphene channel has a low carrier density. The competing interactions between scattering and thermal activation are responsible for the different reduction tendencies. The competition result between Coulomb scattering and acoustic phonon scattering of graphene, and the remote phonon (RP) scattering of substrates/dielectric cause a relatively small decrease of μ at high temperature, which leads to the slight reduction of I_{DS} in the GFETs. In addition, the device maintains almost unchanged DC performance under 200 °C in air ambience for 5 hours, demonstrating the high thermal stabilities for bilayer graphene devices. These results are meaningful and will promote the development of graphene-based devices for practical applications in the future electronics.

References

[1] Geim A K and Novoselov K S 2007 *Nat. Mater.* **6** 183
[2] Morozov S, Novoselov K, Katsnelson M, Schedin F, Elias D, Jaszczak J and Geim A K 2008 *Phys. Rev. Lett.* **100** 016602
[3] Wu Y, Jenkins K A, Valdes-Garcia A, Farmer D B, Zhu Y, Bol A A, Dimitrakopoulos C, Zhu W, Xia F, Avouris P and Lin Y M 2012 *Nano Lett.* **12** 3062
[4] Cheng R, Bai J, Liao L, Zhou H, Chen Y, Liu L, Lin Y, Jiang S, Huang Y and Duan X 2012 *Proc. Nat. Acad. Sci.* **109** 11588
[5] Yu C, He Z Z, Li J, Song X B, Liu Q B, Cai S J and Feng Z H 2016 *Appl. Phys. Lett.* **108** 013102
[6] Yang X Y, Dou X, Rouhanipour A, Zhi L J, Rader H J and Mullen K 2008 *J. Am. Chem. Soc.* **130** 4216
[7] Yan H, Li Z, Li X, Zhu W, Avouris P and Xia F 2012 *Nano Lett.* **12** 3766
[8] Furchi M, Urich A, Pospischil A, Lilley G, Unterrainer K, Detz H, Klang P, Andrews A M, Schrenk W, Strasser G and Mueller T 2012 *Nano Lett.* **12** 2773
[9] Liao L, Bai J, Cheng R, Zhou H, Liu L, Liu Y, Huang Y and Duan X 2012 *Nano Lett.* **12** 2653
[10] Zou K, Hong X and Zhu J 2011 *Phys. Rev. B* **84** 085408
[11] Bolotin K I, Sikes K J, Hone J, Stormer H L and Kim P 2008 *Phys. Rev. Lett.* **101** 096802
[12] Feng T T, Xie D, Li G, Xu J L, Zhao H M, Ren T L and Zhu H W 2014 *Carbon* **78** 250
[13] Yu C, Li J, Liu Q B, Dun S B, He Z Z, Zhang X W, Cai S J and Feng Z H 2013 *Appl. Phys. Lett.* **102** 013107
[14] Yu C, Liu Q B, Li J, Lu W L, He Z Z, Cai S J and Feng Z H 2014 *Appl. Phys. Lett.* **105** 183105
[15] He Z Z, Yang K K, Yu C, Li J, Liu Q B, Lu W L, Feng Z H and Cai S J 2015 *Chin. Phys. Lett.* **32** 117204
[16] Clavel M, Poiroux T, Mouis M, Becerra L, Thomassin J L, Zenasni A, Lapertot G, Rouchon D, Lafond D and Faynot O 2012 *Solid State Electron.* **71** 2
[17] Nyakiti L O, Myers-Ward R L, Wheeler V D, Imhoff E A, Bezares F J, Chun H, Caldwell J D, Friedman A L, Matis B R, Baldwin J W, Campbell P M, Culbertson J C, Eddy C R Jr, Jernigan G G and Gaskill D K 2012 *Nano Lett.* **12** 1749
[18] Tan Y W, Zhang Y, Stormer H L and Kim P 2007 *Eur. Phys. J. Special Topics* **148** 15
[19] Li Q, Hwang E H and Sarma D S 2011 *Phys. Rev. B* **84** 115442
[20] Xu Z, Wang J, Cai Y, Liu J, Yang Z, Li X, Wang M, Yu M, Xie B, Wu W, Ma X, Zhang J and Hao Y 2014 *IEEE Electron Dev. Lett.* **35** 33
[21] Aonar A, Fang T and Jena 2010 *Phys. Rev. B* **82** 115452